

# The Role of Nanoscale Distribution of Fibronectin in the Adhesion of *Staphylococcus aureus* Studied by Protein Patterning and DNA-PAINT

Heba Khateb, Rasmus S. Sørensen, Kimberly Cramer, Alexandra S. Eklund, Jorgen Kjems, Rikke L. Meyer, Ralf Jungmann, and Duncan S. Sutherland\*

Cite This: *ACS Nano* 2022, 16, 10392–10403

Read Online

ACCESS |

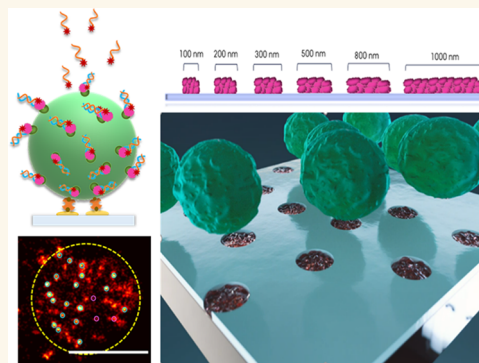
Metrics & More

Article Recommendations

Supporting Information

**ABSTRACT:** *Staphylococcus aureus* is a widespread and highly virulent pathogen that can cause superficial and invasive infections. Interactions between *S. aureus* surface receptors and the extracellular matrix protein fibronectin mediate the bacterial invasion of host cells and is implicated in the colonization of medical implant surfaces. In this study, we investigate the role of distribution of both fibronectin and cellular receptors on the adhesion of *S. aureus* to interfaces as a model for primary adhesion at tissue interfaces or biomaterials. We present fibronectin in patches of systematically varied size (100–1000 nm) in a background of protein and bacteria rejecting chemistry based on PLL-g-PEG and studied *S. aureus* adhesion under flow. We developed a single molecule imaging assay for localizing fibronectin binding receptors on the surface of *S. aureus* via the super-resolution DNA points accumulation for imaging in nanoscale topography (DNA-PAINT) technique. Our results indicate that *S. aureus* adhesion to fibronectin biointerfaces is regulated by the size of available ligand patterns, with an adhesion threshold of 300 nm and larger. DNA-PAINT was used to visualize fibronectin binding receptor organization *in situ* at  $\sim 7$  nm localization precision and with a surface density of  $38\text{--}46 \mu\text{m}^{-2}$ , revealing that the engagement of two or more receptors is required for strong *S. aureus* adhesion to fibronectin biointerfaces.

**KEYWORDS:** protein nanopattern, fibronectin, fibronectin binding protein localization, DNA-PAINT, *Staphylococcus aureus* adhesion, colloidal lithography



Bacterial infections are one of the major concerns in healthcare-associated challenges today.<sup>1–5</sup> *Staphylococcus aureus* is a commensal organism which is carried in the nostrils of 30% of healthy adults,<sup>6</sup> but is a widespread and highly virulent pathogen<sup>7–9</sup> that can cause superficial and invasive infections.<sup>10,11</sup> *S. aureus* has been isolated from infections of damaged tissue or implanted materials<sup>12</sup> and is considered as a dominant cause of acute infective endocarditis<sup>13</sup> with associated mortality rates of 20%–40%. Staphylococci were identified in the majority (nearly 80%) of prosthetic implant-associated infections,<sup>14,15</sup> where in orthopedic infections *S. aureus* and *Staphylococcus epidermidis* together account for two out of three cases.<sup>15</sup>

The pathogenicity of *S. aureus* is caused by a broad range of virulence factors<sup>16–18</sup> including cell wall anchored proteins used for attachment to the host.<sup>19–22</sup> The microbial surface component recognizing adhesive matrix molecules

(MSCRAMMs) mediate attachment of *S. aureus*<sup>23,24</sup> to host ECM proteins, such as collagen, fibrinogen, and fibronectin (Fn)<sup>25</sup> as a required first step in biofilm formation, e.g., on the surface of medical implants. Adhesion to Fn also promotes internalization of *S. aureus* by mammalian cells.<sup>25–29</sup> Like biofilm formation, internalization by nonphagocytic host cells is an important mechanism to avoid detection by the host immune system.<sup>30</sup>

*S. aureus* interacts with Fn using several MSCRAMMs, such as FnBPA and FnBPB<sup>25</sup> and Ehb, Emb, and Aaa.<sup>31</sup> Fibronectin has

Received: January 19, 2022

Accepted: July 5, 2022

Published: July 8, 2022



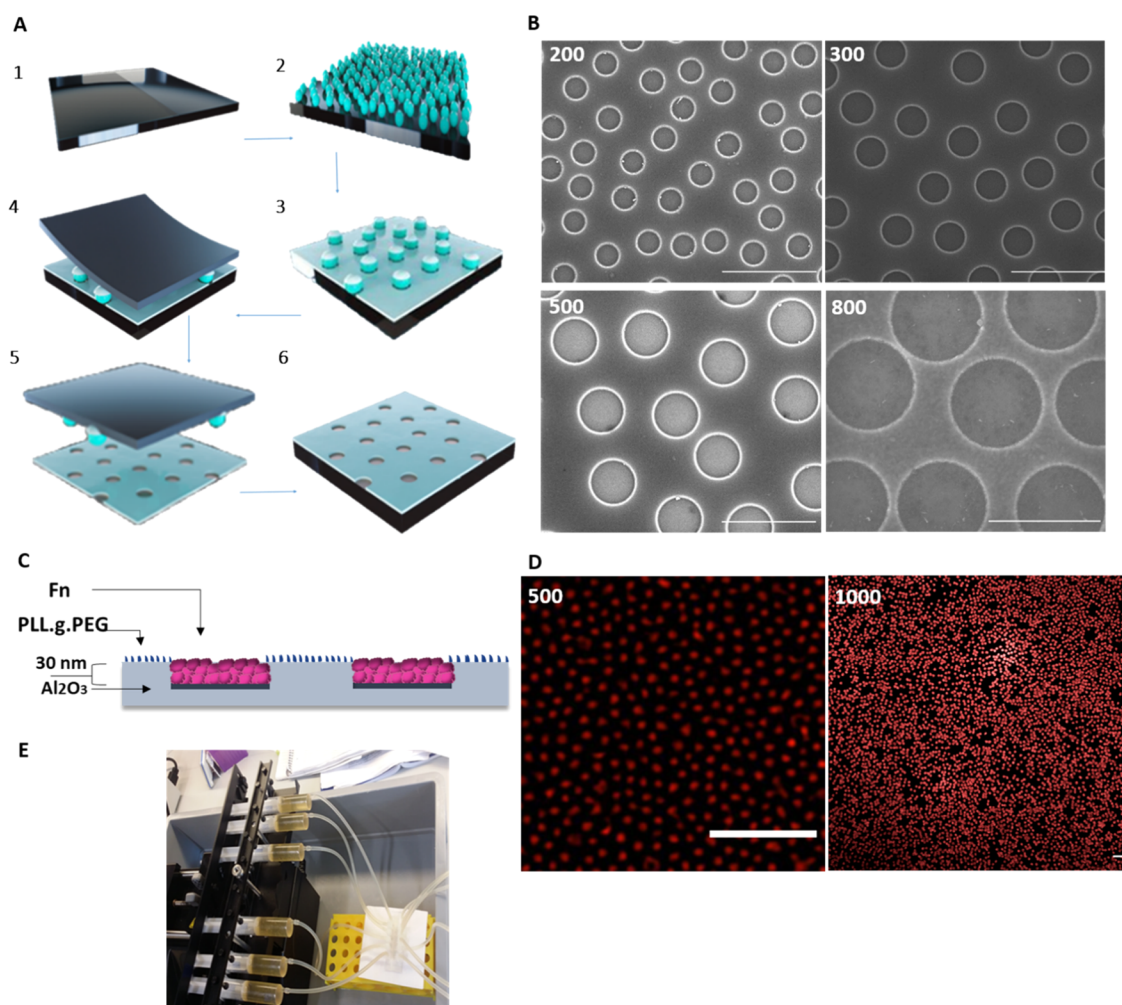


**Figure 1.** Schematic representation illustrating the generation of a series of protein patterns. (A) (1) Al (3 nm) precovered glass substrate. (2) Self-assembled polystyrene nanoparticle mask. (3) 2 nm Ti and 30 nm SiO<sub>2</sub> deposited onto the surface. (4 and 5) Particle mask removed by taped stripping. (6) Al<sub>2</sub>O<sub>3</sub>/SiO<sub>2</sub> patterned substrate. (B) SEM images of holes with diameters of 100, 300, 500, and 800 nm (scale bars: 1 μm). (C) Schematic sideview Fn/PLL-g-PEG nanopatterns. (D) Immunofluorescence of Fn patterns, 500 nm pattern (left, SIM image) and 1000 nm pattern (right, CLSM image) (scale bars: 5 μm). (E) Image of the used flow system.

multiple bacterial binding domains at the N-terminal, which contains five sequential (1–5) Fn type 1 modules.<sup>32</sup> FnBPs contain multiple nonidentical fibronectin binding regions (FnBr) binding specifically to type 1 Fn modules in up to 11 binding repeats (FnBPA with 11 repeats and FnBPB with 10 repeats).<sup>32,29</sup> Increased avidity of the interactions between multiple FnBr domains in individual bacterial surface proteins and Fn bound at surfaces, or in solution, plays a role in increasing bacterial adhesion<sup>25,33</sup> and can mediate interactions with integrins at the surface of mammalian cells. The interaction forms an extended tandem  $\beta$ -zipper bound to multiple Fn type 1 domains on one or more Fn molecules.<sup>32,34</sup> While there has been a significant research effort to understand the role of the FnBr domains in individual FnBPs in mediating receptor binding, much less focus has been placed on the local distribution of MSCRAMMS at the bacterial surface and of the ligands (e.g., Fn) on the surface to which it adheres.<sup>23</sup> Fibronectin and other ECM proteins have been widely studied in relation to biomaterials due to their important role in influencing cell behavior around biomedical implants,<sup>35</sup> highlighting that the loss of Fn-binding proteins reduced the cell adhesion onto surfaces during the primary adhesion<sup>36,37</sup> and a key finding has

been the critical importance of nanoscale organization of specific proteins such as Fn, Vn, and Ln on the adhesion, signaling, and differentiation of mammalian cells,<sup>38–40</sup> particularly when the patterns are on length scales well below that of the cells. Multiple mechanisms of altered interaction have been proposed from minimum ligand spacings,<sup>41,42</sup> minimum ligand numbers, or patch areas.<sup>43,44,38</sup> While there is a significant body of work investigating eukaryote interactions, to date no similar investigations have been carried out for the role of ECM protein patterns on prokaryote adhesion. Exploring and understanding the relevant length scale of distribution of Fn binding proteins<sup>45</sup> at the bacterial surface and Fn availability at a biointerface will provide a molecular insight into the primary adhesion of *S. aureus* at the inhomogeneous surfaces of medical implants or organized ECM in host tissues. A clear challenge when studying prokaryotes comes from their small size where application of traditional wide-field and confocal fluorescence microscopes (with diffraction limited resolutions in the range 250–500 nm) to the study at subcellular dimensions becomes difficult. To date, there are no fluorescence studies showing the distribution of FnBP receptors at the surface of *S. aureus*.

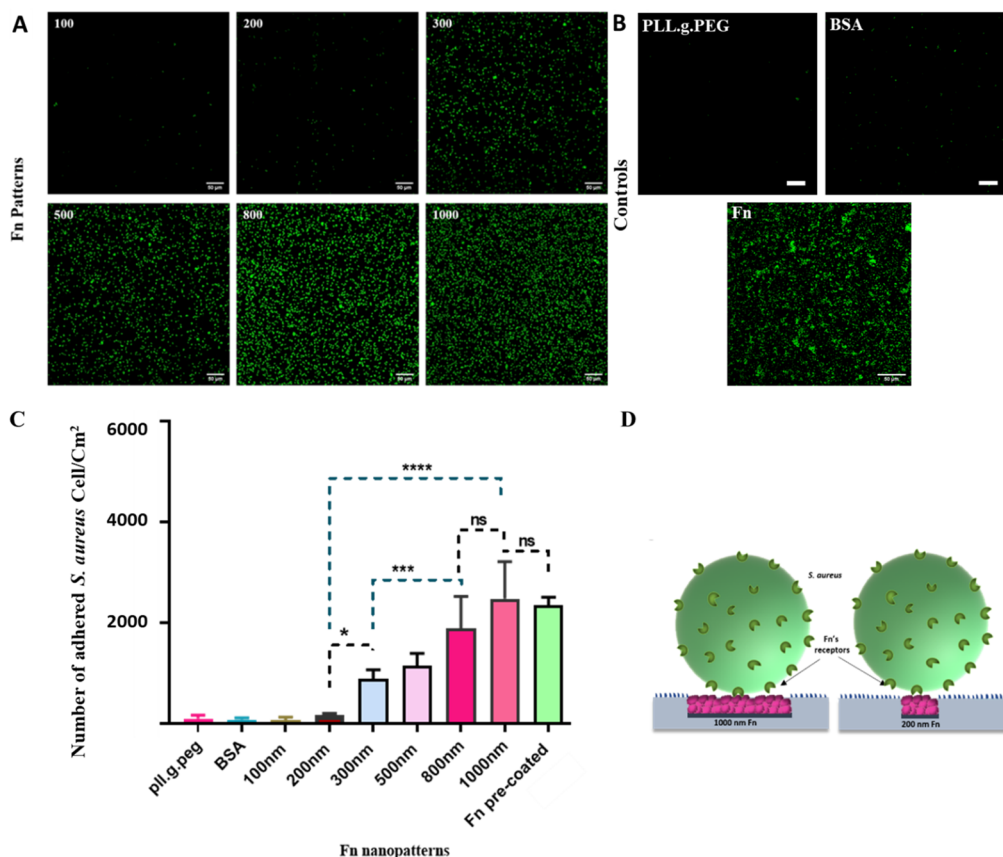


**Figure 2.** (A) Representative CLSM images of the *S. aureus* adhesion to Fn patterns (nominal diameters (nm) indicated). (B) Control measurements for *S. aureus* adhesion to glass surfaces coated with PLL-g-PEG, BSA, and Fn (scale bar 50  $\mu\text{m}$ ). (C) Number of bacterial cells/mm<sup>2</sup> on different Fn nanopattern compared to controls surfaces. Bars show mean  $\pm$  s.d. of five independent experiments. <sup>(n.s.)</sup> $p < 0.5$ ,  $*p < 0.05$ ,  $**p < 0.01$ ,  $***p > 0.001$ ,  $****p < 0.0001$ . (D) Schematic representation of *S. aureus* interaction with Fn patches of different size.

Advances in super-resolution imaging in the past decade have enabled fluorescence microscopy approaches to provide spatial information characterizing cellular structures far below the diffraction limit. These methods include stimulated emission depletion microscopy,<sup>46</sup> photoactivated localization microscopy,<sup>47</sup> single-molecule localization microscopy,<sup>48,49</sup> and stochastic optical reconstruction microscopy.<sup>50</sup> These techniques all rely on switching molecules between on and off fluorescence states to obtain subdiffraction limit image resolution, but suffer from bleaching effects limiting the resolution and applicability of these approaches. A recently developed approach called DNA points accumulation for imaging in nanoscale topography (DNA-PAINT)<sup>51</sup> overcomes this limit by utilizing transiently binding fluorescent probes through weak DNA–DNA interactions, or more recently, peptide coil–coil interactions,<sup>52</sup> to provide robust single molecule localization<sup>23–28,52</sup> with few nanometer resolution.

In this study, we investigated the role of Fn surface distribution for the adhesion of *S. aureus* to interfaces as a model for primary adhesion at tissue interfaces or protein covered biomaterials by applying nanopatterning and super-resolution microscopy techniques. We presented Fn in patches of varying size (100–1000 nm) in a background of protein and bacteria rejecting chemistry based on PLL-g-PEG and studied primary adhesion of *S. aureus*. A clear role for protein patch size in controlling adhesion was observed with a threshold for adhesion requiring Fn patches larger than 200 nm. The range of Fn pattern sizes studied went from a pattern comparable to the

size of the bacterium ( $\sim 1 \mu\text{m}$ ) down to close to the size scale of individual receptors ( $\sim 20\text{--}50 \text{ nm}$ ). To visualize Fn binding receptor distributions on bacterial cells at super resolution, we developed the DNA-PAINT technique. Here, oligonucleotide-labeled Fn was used as an imaging probe for Fn binding proteins in the membrane of wild-type *S. aureus*. The measured receptor density suggests that the adhesion of *S. aureus* requires the engagement of multiple FnBPs for strong adhesion rather than single high-affinity interactions.

## RESULTS AND DISCUSSION

Developments in the field of nanotechnology have enabled new approaches to study topics such as cellular adhesion via both fabrication approaches to define materials with nanoscale organization and new tools to characterize at the nanoscale. Here, we have developed and utilized colloidal lithography techniques<sup>53</sup> combined with site-specific material modification to generate a series of protein patterns of Fn on transparent substrates to explore the role of ligand organization on *S. aureus* adhesion. In parallel, we have applied the super-resolution imaging approach DNA-PAINT<sup>54,55</sup> to visualize the distribution of Fn receptors on the surface of *S. aureus*.

**Nanopatterned Fibronectin.** Materials with defined nanoscale distributions of Fn on transparent substrates were prepared for use in bacterial adhesion studies in microfluidic channels. Sparse colloidal lithography<sup>56</sup> was used to prepare glass cover slides with surface chemistry defined regions of protein rejecting (PEG-based) or protein binding character and

used to direct the physical adsorption of Fn into circular patterns of size 100 nm up to 1000 nm. These cover slides could be attached to commercial fluidic channels and used in studies of bacterial adhesion under flow.

Dense short-range ordered arrays of circular domains of Al<sub>2</sub>O<sub>3</sub> chemistry in a background of SiO<sub>2</sub> were produced using dispersed colloidal monolayer masks. The process is schematically shown in Figure 1A. In brief, glass cover slides (60 μm thick) were coated with 3 nm-thick aluminum layers by physical vapor deposition (PVD) and fully oxidized by oxygen plasma to produce a transparent aluminum oxide layers which gave the surface a positive charge at neutral pH. Negatively charged sulfate-modified polystyrene nanoparticles were allowed to adsorb to the surface from dilute aqueous solution to form a complete dispersed short-ranged ordered monolayer where the distribution is well described by random sequential adsorption<sup>53</sup> with a characteristic spacing but no long-range order. The distribution of particles is maintained during drying by using a predrying heating process to raise the particles above the glass transition for the polymer (heated to >120 °C in a pressure chamber) to increase the surface interaction and prevent capillary-force induced aggregation. Thereafter, a 30 nm silicon dioxide layer with a 2 nm titanium adhesion layer was deposited by PVD, and the particles were removed by tape stripping to reveal alumina patches with the diameter of the particles. In a final step, the sample was cleaned with oxygen plasma before use. Scanning electron microscopy (SEM) was used for characterization and verification of a range of the different hole sizes. Figure 1B shows different nanopatterns with circular Al<sub>2</sub>O<sub>3</sub> domains in a background of SiO<sub>2</sub> (a wider range of nanopatterns is shown in Figure S1). We confirmed the full oxidation of the aluminum layer and the stability of the layer after exposure to media by XPS (see Figure S1). The SiO<sub>2</sub> regions were subsequently chemically modified with PLL-g-PEG by the electrostatic assembly to prevent nonspecific protein adsorption to the background regions. The positively charged PLL backbone adsorbs strongly to negatively charged metal oxides, forming a dense brush of PEG extending from the surface. For this polymer under these conditions, the amount of protein binding is reduced by >97%.<sup>57</sup> The positively charged (at neutral pH) alumina surface prevents adsorption of the PLL groups, meaning that while protein is prevented from adsorbing to the silica surface after PLL-g-PEG treatment, protein can readily adsorb to the alumina surface. Fibronectin was allowed to adsorb to the surface and defined into patterns or onto homogeneous surfaces by adhesion to the Al<sub>2</sub>O<sub>3</sub> surfaces (Figure 1C). High-quality protein patterns of Fn were successfully demonstrated by immunofluorescence (Figure S2) and (Figure 1D). Patterns of proteins have previously been formed in this way at gold/silica surfaces where the gold had been modified to be hydrophobic<sup>43</sup> or positively charged.<sup>58</sup> Here, they are prepared on fully transparent substrates.

**Bacterial Adhesion.** The nanopatterned samples together with homogeneous surfaces were mounted on Ibidi sticky slide slides with 6 channels per slide. Chemical functionalization and protein deposition were carried out within the channels, and the final patterns were washed with buffer before exposure to a 0.15 μL/min flow of *S. aureus* (optical density at 600 nm (OD<sub>600</sub>) of 0.1) for 30 min (Figure 1E). Each channel on a sample was exposed to independently grown bacterial cultures to account for biological variation. After rinsing with PBS for 10 min with the same flow rate, the attached bacterial cells were stained with SYBR Green I from Invitrogen and imaged by confocal laser

fluorescence microscopy (CLSM). Control measurements with different surface treatments were carried out, so several surfaces, precoated with BSA or PLL-g-PEG, were exposed to a flow of bacterial cells. Representative fluorescence images are shown in Figure 2A,B. Five independent experiments were carried out for each fabricated surface, and five random regions were imaged for each experiment.

There was no significant bacterial attachment to Fn-coated surfaces with the 100 and 200 nm pattern sizes compared to the Fn-free negative control surfaces coated with either PLL-g-PEG or BSA (Figure 2). An increasing number of bacteria attached to Fn-coated surfaces with larger size of Fn patches from 300 nm patches and up. At the largest patch sizes (800 and 1000 nm), bacterial attachment was comparable to the homogeneous Fn samples, even though the amount of Fn on homogeneous samples was 3 fold higher (Table S1).

The cells were counted using ImageJ software. The database was analyzed by (Graph-Pad Prism, 8). The data in (Figure 2C) shows a comparison between the numbers of attached *S. aureus* on different Fn nanopatterns and control samples. The variation between the replicates is plotted as a standard deviation between the means from each channel. A threshold for bacterial attachment appeared between 200 and 300 nm-sized patches, with a significant but intermediate number of bacteria seen at 300 nm surfaces which in general increases as the pattern size increases. No difference is seen between 800 or 1000 nm samples and the homogeneous surface, despite there being approximately 3 times more Fn-coated area available for binding at the homogeneous surfaces (Table S1), which indicates that it is not the global protein available that is important, but the locally available ligands. The global coverage of ligand for the 200 and 300 nm samples is similar (18% vs 24%); however, we cannot rule out that the increased global coverage plays a role in the increasing binding seen from 300 nm up to 1000 nm. Bacteria can in many situations adhere strongly to materials surfaces through nonspecific interactions. Here, the polymeric (PLL-g-PEG) and protein coatings are intended to reduce nonspecific interactions. For the functionalized surfaces, essentially no adherent cells are seen at the PLL-g-PEG surface indicating that chemistry successfully prevents bacterial attachment under these conditions. Similarly, no binding was seen at BSA-coated glass surfaces, which indicate that protein layers could mask the underlying chemistry and limit nonspecific interactions and that the binding observed to Fn patterns required Fn.

The protein patterns formed here were made from chemically nanostructured materials formed from holes that were 32 nm deep (30 nm SiO<sub>2</sub> and 2 nm Ti). Fibronectin is expected to form a maximum of 15–20 nm-thick layers so will not have extended above the silica surface, although bacterial receptors can likely extend into the holes. To explore if the aspect ratio (diameter/height) of the holes, which was lower for the smaller diameter holes compared to the larger diameter holes, influenced the results, experiments were carried out for 15 nm-thick silica layers for the 200 nm diameter patterns which showed similar low levels of binding (Figure S4), indicating that the threshold seen between 200 and 300 nm was not caused by any steric effects. A conclusion from the experimental results is that *S. aureus* requires a Fn patch area larger than 200 nm for significant strong interactions.

*S. aureus* binds to Fn via the cell wall anchored FnBP's using a tandem β-zipper mechanism.<sup>25,32,29</sup> Interestingly, it has been found that low binding affinity of FnBPs results when binding to

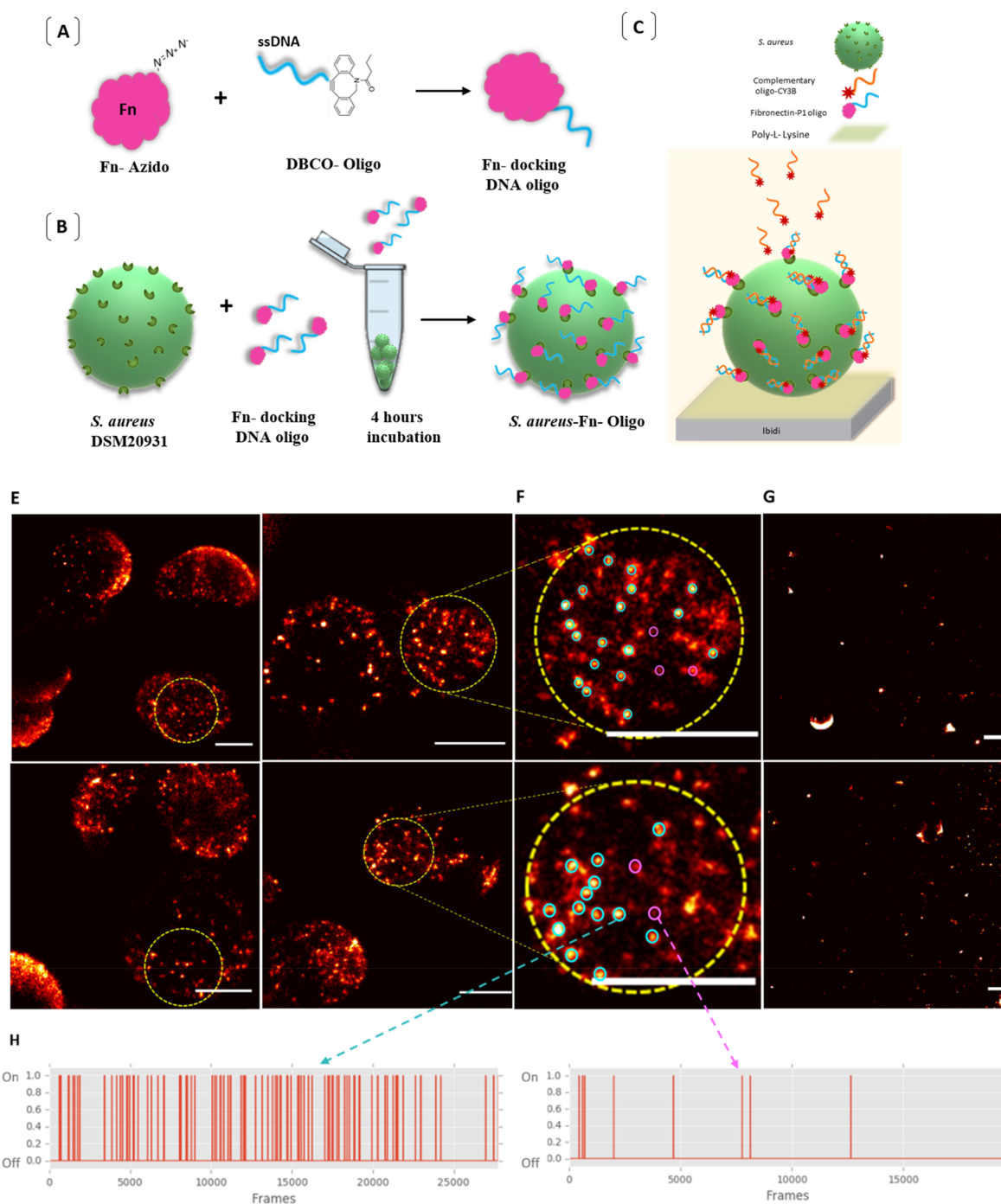


**Figure 3.** Characterization of FnBPs on *S. aureus* single cells using DNA-PAINT. (A) Schematic diagram depicting the functionalization of Fn with PS3 DNA-PAINT docking strand. (B) Diagram illustrating the binding of Fn at the surface of *S. aureus*. (C) Schematic diagram depicting the approach for cell immobilization via PLL and single-molecule localization of FnBPs at single *S. aureus* bacteria via an imager DNA strand. (D) DNA-PAINT super-resolution images visualizing the localization of FnBPs on single *S. aureus* bacteria. The highlighted areas correspond to  $\sim 0.36 \mu\text{m}^2$ . (E) Zoom-in of highlighted areas shows examples of the localized spots in cyan and of unspecific background features in magenta. Image resolution: 39 nm (scale bars: 500 nm). (F) Negative control of the complementary DNA-PAINT imager strands PS3\* added onto bare immobilized *S. aureus* cells lacking the Fn-docking strand PS3 (scale bars: 500 nm). (G) Time traces of spots with repetitive binding events in cyan (left) and of unspecific background features in magenta (right).

individual short type 1 Fn modules, in contrast to neighboring arrayed Fn type 1 domains which result in high affinity, implying that avidity plays an important role.<sup>59</sup> In studies carried out with mammalian cells, ligand spacing, ligand number, and area of ligand patch were all seen as important for determining the cellular adhesion. Here, the density of ligands at the surface is

high, but the density of Fn ligands at the surface of the bacteria may be limited.

The curvature of the outer wall of *S. aureus* (around  $1 \mu\text{m}$  in diameter) will make it likely that each bacterium interacts with a single or, at most, a few patches. The contact region of *S. aureus* at material surfaces has been estimated to be in the range of

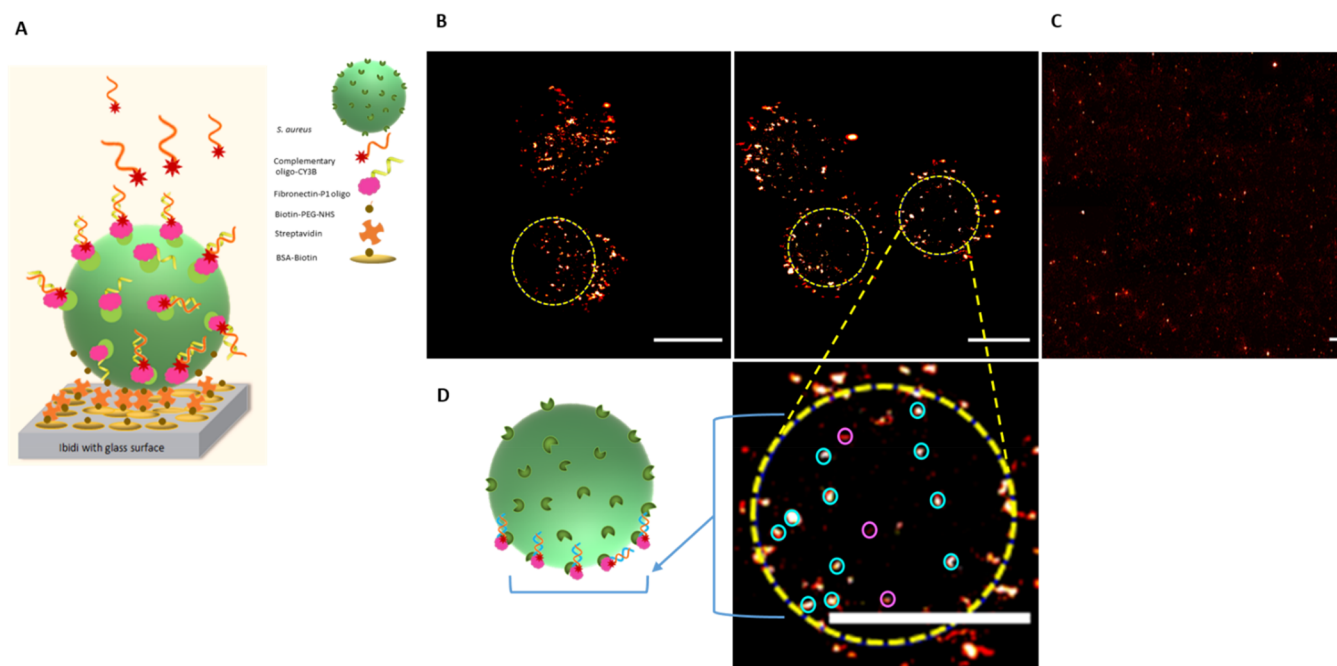


**Figure 4.** Characterization of FnBPs onto *S. aureus* single cell via DNA-PAINT. (A) Schematic diagram of the tethering approach and imager strand localization. (B) DNA-PAINT images at  $\sim 8$  nm super-resolution visualizing the localization of FnBPs at *S. aureus* cells (scale bars: 500 nm). The highlighted areas show  $\sim 0.31 \mu\text{m}^2$ . (C) Negative control of the complementary DNA-PAINT imager strands R3\* added onto the bare immobilized *S. aureus* cell lacking the Fn-docking strand R3 (scale bars: 1000 nm). (D) (left) Schematic representation illustrating the region of the cell analyzed; (right) zoom-in of the bottom of the cell. Examples of the localized spots in cyan and of unspecific background features in magenta (scale bars: 500 nm).

200–300 nm in diameter when interacting via nonspecific interactions.<sup>60</sup> Figure 2D shows a schematic that represents the relative sizes of the *S. aureus* bacteria and patches. Only adhesion receptors on the *S. aureus* surface which are close to the contact region are likely to be able to bind to the Fn. The different nanopatterned surfaces present slightly different global areas of Fn ( $\sim 12\%$  for 100 nm structures and  $\sim 36\%$  for 1000 nm structures see Table S1 and Figure S3). However, this difference in global presentation is unlikely to provide the experimental outcome first because the 1000 nm structures give the same adhesion as the homogeneous Fn surfaces which have 100% coverage and  $\sim 3$  times higher area available, and second because the 200 and 300 nm surfaces on either side of the threshold for adhesion have similar global coverage of Fn  $\sim 18$  and 22% respectively. By contrast, the local coverage will play a role in that a bacterium that lands within a 1000 nm patch has likely a sufficiently large area available to accommodate all the FnBPs that can reach the surface, while the smaller patch sizes will restrict access to Fn for some of these FnBPs and thus the number of FnBPs that can be engaged, since the local area of available Fn will be reduced. The number of Fn molecules available in a 200 nm patch is likely already quite large ( $>100$  Fn's) which should be compared to the  $\sim 6$ – $8$  Fn molecules that are estimated to be able to bind to an individual FnBPA protein<sup>61</sup> so there are easily sufficient ligands to engage with many individual FnBP's within a single patch. While there are high numbers of Fn molecules within a patch, there must be FnBPs to interact with them. We hypothesize that the threshold behavior of adhesion with Fn patch size results from a threshold number of FnBPs being required to give sufficient adhesive strength to keep the bacterium at the surface in our conditions (under flow). The concentration of FnBPs at the surface of *S. aureus* would provide a finite number of ligand binding

molecules that would be available above an individual Fn patch. We propose that the number of FnBPs able to interact with the surface falls below a critical threshold for 200 nm patches, meaning that bacterial attachment becomes too weak to keep the bacterium at the surface. To examine this assumption, we localized the Fn receptors on single *S. aureus* cells via the super-resolution imaging approach, DNA PAINT.

**FnBP Localization.** Since *S. aureus* has several different fibronectin binding proteins (FnBPA and FnBPB), we developed a single-molecule binding assay utilizing Fn as the readout probe for the localization of Fn binding proteins. Using DNA-PAINT, we achieved images with localization precision (NeNA) down to 7 nm.

In this assay, Fn conjugated to a DNA-PAINT docking sequence (PS3 or R3) was used as a readout for FnBP localization. Thus, transient binding of the PS3 or R3 extension using complementary Cy3B-labeled imager strands enabled single-molecule imaging and localization.

Fibronectin was labeled with DNA-PAINT docking sequences (PS3 or R3) via a click-chemistry reaction. First, the Fn was functionalized with NHS-PEG4-azide groups followed by linking the azide with DBCO-oligos for the conjugation with the DNA-PAINT docking strand (Figure 3A, Figure S5). The Fn is likely functionalized with 3–5 docking strands which increased sampling and thus overall image quality.

In order to image bacterial cells with DNA-PAINT, the cells must be tethered to a surface with sufficient mechanical stability. The final image is based on the overlay of thousands of frames, meaning that any undesirable cell mobility can significantly reduce the image quality and reconstruction fidelity. Two different immobilization assays were explored in this study to overcome the significant challenge of holding the spherical cells stationary while limiting background fluorescence. In the first

assay, 0.01% poly-L-lysine (PLL) was used to coat a coverslip surface for 30 min. Thereafter, the fixed cells were added to the 6-channel 400  $\mu\text{m}$  height (IV 0.4) ibidi flow chambers, subsequently centrifugation of the ibidi slide at 3700 rpm<sup>62</sup> was applied, and the nonimmobilized cells were removed with PBS washing steps (Figure 3C). DNA-PAINT was then performed using 5 nM Cy3B-labeled complementary imager strands of PS3. The fluorescence emission upon binding was detected using highly inclined and laminated optical sheet microscopy.<sup>63</sup> This enabled imaging of horizontal slices of the bacteria slightly above the glass slide surface. A challenge with the use of PLL was background fluorescence from the PLL-coated glass surface, which could be avoided by imaging the bacteria in a plane above the surface. Some of the bacteria in this protocol appeared to be suspended above the surface apparently attached to other cells. Only cells appearing roughly in the lower 200 nm from the glass surface were considered for further quantification purposes (Figure 3D).

Intensity vs time traces for each apparent cluster of binding events were analyzed for repetitive binding, subsequently retained for further data quantification (while rejecting non-specific events). Specific areas of  $0.36 \mu\text{m}^2$  were analyzed from multiple cells, and the average number of bound Fn molecules were quantified to estimate the FnBPs localization (Figure 3E). We assume that all FnBPs have a bound Fn so this represents a lower limit. Images of *S. aureus* cells without preincubation with the Fn for the same conditions were taken, and only few, mostly unspecific binding sites, were observed (Figure 3F). A comparison between traces of an identical localizing point (G, left) and unspecific background features (G, right) in time shows a significant difference through the imaged frames.

The second cell immobilization protocol we developed relied on tethering the cells onto the bottom of ibidi chamber slides via biotin–streptavidin binding, to avoid the fluorescent background observed with PLL and thus resulting in increased image quality (Figure 4). Briefly, the cells were reacted with the functionalized fibronectin Fn-R3, and before fixation, the cells were biotinylated with NHS-dPEG<sub>4</sub>-biotin. Ibi chambers with glass slides were prepared by precoating them with BSA-biotin followed by streptavidin before exposure to the biotinylated *S. aureus* (Figure 4A). DNA-PAINT imaging was performed at the surface of the bacteria close to the coverslip, near total internal reflection conditions. The biotin-streptavidin immobilization method generally demonstrated better mechanical stability with reduced fluorescence background (Figure 4B). The DNA-PAINT images using this bacterial immobilization protocol reached a significantly better localization precision (NeNA) of 7 and 9.3 nm, compared to 12.8 and 15 nm for the immobilization approach based on PLL. The binding quantification was estimated in an identified area of  $0.31 \mu\text{m}^2$  at each image from multiple cells (Figure 4B).

The density of FnBPs receptors was estimated on six *S. aureus* cells from three independent experimental sets using two different imager strands of PS3 or R3, giving  $\sim 38$ – $46$  receptors per  $\mu\text{m}^2$  area and an average number of FnBPs on a single cell of  $\sim 130$  receptors. Lower et al.<sup>64</sup> utilizing force spectroscopy with Fn functionalized AFM tips proposed 36 FnBP's per  $\mu\text{m}^2$  (around 110 per bacterium) for *S. aureus* adsorbed to Fn-coated glass, which is in good agreement with our findings. Here, the studied bacteria were in stationary phase, adhesion studies in an in vivo situation have shown higher rates of adhesion, and a higher surface density of FnBPs for *S. aureus* during the exponential phase compared to stationary phase may be

expected.<sup>65</sup> In this bacterial adhesion study, the limiting area of Fn available in a single patch will have limited the number of FnBPs able to engage with Fn bound to the surface. Geometric considerations indicate that for 130 receptors per bacterium, there are on average  $\sim 1.2$ – $1.4$  FnBPs available per 200 nm patch of Fn, at which condition we did not see any adhesion. The 2.25 times larger 300 nm patches would have provided access to  $\sim 2.7$ – $3.2$  FnBPs. These data suggest that a minimum of two or three FnBP molecules were needed to give sufficient binding strength for attachment under flow conditions. Since the distribution of FnBPs was not homogeneous and the binding increased with increasing Fn patch size above 300 nm, a larger number of interacting FnBP's are likely required for stronger adhesion. We suggest that the limiting factor for adhesion of *S. aureus* on 100 and 200 nanopatterns of Fn is due to the density of FnBPs at the cell surface, largely limiting the interaction to single FnBPs, and that single FnBP engagement was not enough to provide strong binding.

Interestingly, the lack of *S. aureus* binding to Fn nanopatterns to patterns below 300 nm can be compared to mammalian cell adhesion to similar-sized patterns, where epidermal stem cells show adhesion already from 100 nm patterns,<sup>38</sup> to help shape the future of bioconstructive materials that can promote tissue integration but prevent bacterial colonization.

## CONCLUSION

In this work, we have applied advanced nanoscale fabrication and characterization approaches to study *S. aureus* adhesion to ECM. We investigated the interaction of *S. aureus* with nanoscale distributions of Fn prepared by colloidal lithography. We observed a threshold behavior in adhesion of *S. aureus* to nanoscale distributions of Fn with minimal adhesion to patches with diameters up to 200 nm. DNA-PAINT characterization of distributions of Fn binding proteins at the surface of *S. aureus* suggested that the threshold behavior in adhesion resulted from too few receptors being available above individual patches. Geometric considerations indicated that engagement of more than one FnBP with surface bound Fn is required for strong adhesion. These results provide insight into bacterial adhesion to the extracellular matrix and to the design of biomedical implant material surfaces promoting cellular adhesion but limited bacterial adhesion. The methods developed and demonstrated in this work with *S. aureus* can have application to study a broad range of bacterial interactions with ECM and mammalian cell membrane proteins.

## MATERIALS AND METHODS

**Materials.** Poly(dimethylammonium chloride) (PDDA) and poly-(sodium-4-styrenesulfonate) (PSS) were purchased from Sigma-Aldrich (DK). Polyammonium chloride (PAX-XL60) was purchased from Kemira Miljo (DK) and sulfate modified polystyrene colloidal particles in water were purchased from Invitrogen. *S. aureus* DMS 20231 was purchased from DSMZ, Germany. Human fibronectin protein was purchased from R&D systems (USA). All standard DNA oligonucleotides DBCO-PS3d, DBCO-R3, PS3i-CyB3, and R3-CyB3 sequences were purchased from IDT (DK). DBCO-NHS A124 was obtained from the click chemistry tool. PLL P8920, streptavidin 189730, biotin-NHS H1759-5MG, glycin50046, TBE buffer T4415-1L, and TSB medium were obtained from Sigma-Aldrich (DK). Biotin-BSA 29130 and SDS-PAGE (EA03552BOX) were obtained from Thermo Fisher. NHS-dPEG<sub>4</sub>-biotin (BD1-A0401-045) from quantabiodesign (USA).  $\mu$ -Slide VI 0.4 and ibidi  $\mu$ -slide VI 0.5 glass bottom channel slide cat. no. 80607 from ibidi (DK). NHS-PEG4-azide (CLK-AZ103-100) was obtained from Jena bioscience (DE).

**Methods. Sparse Colloidal Lithography.** Monolayers of adsorbed dispersed colloidal nanoparticles were used as masks for pattern transfer by PVD as described previously.<sup>44</sup> Negatively charged colloidal particles (sulfate modified polystyrene) were deposited on oppositely charged substrates by electrostatic self-assembly. The substrates (glass coverslides with thin aluminum oxide overlayers) were given a stable positive charge by sequential deposition of three different charged polyelectrolyte layers PDDA, PSS, and PAX in an aqueous solution where the third layer had a positive charge at neutral pH. Colloidal particles of different sizes 100–1000 nm were used to form transparent chemical patterns of aluminum oxide/silicon dioxide. Later exposure to PLL-g-PEG could direct the PLL-g-PEG to the silicon dioxide parts of the surface.

The process of formation of hole patterns is shown in Figure 1. Glass substrates of size 25 × 60 mm were cleaned with acetone followed by oxygen plasma cleaning, 100 W, 25 mTorr for 15 min (Vision 300 Mark II, Advanced Vacuum AB Sweden). A thin layer of aluminum was deposited onto the surface via physical vapor deposition (electron beam stimulated thermal evaporation, Cyrofox GLAD, Polyteknik A/S DK, 0.1 nm/s base pressure <10<sup>-7</sup> Torr), which is used later for creating positively charged aluminum oxide regions to electrostatically repel PLL-g-PEG and interact with the adsorbing protein. Different layers thicknesses were examined in terms of stability with different buffer treatments and also transparency. Therefore, a 3 nm aluminum layer was chosen which was then oxidized to form aluminum oxide (alumina) by exposure to oxygen plasma (50 W, 25 mTorr for 2 min) (Figure 1A). The surface was coated with three sequentially deposited polyelectrolyte layers (PDDA, PSS, PAX). Electrostatically charged (negative) particles adsorb directly onto the opposite charged (positive) surface (Figure 1B). Colloidal monolayers of charged polystyrene particles with different diameters were formed (100, 200, 300, 500, 800, 1000 nm using bulk nanoparticle concentrations of 0.2% volume for the three smallest diameters, 0.5% for 500 nm, 1% for 800 nm, and 2% for 1000 nm) by assembly onto a preformed triple layer of polyelectrolytes. After the particle deposition (2 min for 100 and 200 nm particles and overnight for 300–1000 nm particles), the samples were carefully rinsed, followed by transfer into a pressure chamber containing deionized water which was then heated to 120 °C to increase nanoparticle adhesion to the surface in order to prevent aggregation during subsequent drying. The coating process of the pretreated glass samples continued with the deposition of 2 nm Ti and 30 nm of SiO<sub>2</sub> in the same process run (Ti deposition rate 0.02 nm/s, SiO<sub>2</sub> deposition rate 0.1 nm/s, base pressure <10<sup>-7</sup> Torr) by PVD (Figure 1C). The particles were removed by tape stripping followed by oxygen plasma cleaning (50 W, 25 mTorr for 10 min) (Figure 1E). Afterward, samples were rinsed with acetone, ethanol, and deionized water, respectively, under sonication until any remaining particles were removed. The samples were then dried under a stream of nitrogen gas followed by cleaning for 30 min in UV/ozone. SEM was used for characterization of the samples to determine holes size, surface coverage, and interhole distances from 4 images per sample type (50K magnification for 100 nm structures and 10K magnification for the other structure sizes).

**Fibronectin Nanopatch Preparation.** The fabricated surfaces with patterns of different diameters were sterilized in 70% EtOH. Then the samples were attached to ibidi chambers. Thereafter, 100 μL of 0.25 mg/mL PLL-g-PEG in 10 mM HEPES pH 7.4 was injected into each chamber and heated to 60 °C for 30 min. The surfaces were rinsed with HEPES (10 mM) and Tris buffer (2.7 Mm), respectively, and then incubated with bovine Fn (1030-FN, R&D Biotech) 20 μg/mL in Tris buffer (2.7 mM) overnight. Next day, the samples were rinsed with Tris buffer, followed by blocking for unspecific binding with 2% BSA in Tris buffer for 30 min at room temperature. Then, the surfaces were washed with Tris buffer and used immediately.

**Flow Experiment.** A colony of *S. aureus* DSM 20231 was inoculated into tryptic soy broth and incubated overnight at 37 °C with gentle shaking (130 rpm). Whole genome analysis of this strain showed the presence of the genes for the fibronectin binding protein FnBPA, FnBPB, and Ebb and the fibrinogen binding proteins ClfA and ClfB.<sup>66</sup> Five independently grown cultures were prepared for each experiment. The bacteria concentration was adjusted with fresh media to an OD of

0.1 at a wavelength of 600 nm which corresponds to ~5 × 10<sup>7</sup> CFU/mL.

The adjusted cultures were inserted into a syringe pump to which the ibidi chamber was connected. The flow was adjusted to 0.15 μL/min for 30 min followed by rinsing with PBS for 10 min at the same flow rate (shear stress ~1.8–1.9 μdyn/cm<sup>2</sup>). The remaining bacterial cells were stained with SYBR Green I 1× working concentration according to manufacturers instructions.

**Microscopy and Data Analysis.** The adhered cells were imaged in PBS using by CLSM (Zeiss LSM700), 20× Plan-Neofluoar and 63× Plan-Apochromat NA1.4 objective, using 488 nm excitation. At least 5 images were taken for each ibidi channel for each of the sample types. Images with 20× magnification were randomly chosen in each of the ibidi channels, whereas the 63× magnification images were manually chosen as representative of the population on the surface. The number of bacterial cells was determined with ImageJ software using the particle count protocol. Prior to the automatic analysis, a color threshold was set manually for the images.

**Statistical Analysis.** One-way analysis of variance was performed for the difference between the number of adhered cells onto each Fn patch size, followed by Tukey's test for multiple comparisons using (Graph-Pad Prism,8) to visualize the significant differences at the 0.05 level.

**Immunofluorescence of Fibronectin.** Primary antifibronectin antibody (anti-Fn1 antibody produced in rabbit, AV41490 Sigma) was diluted 1:500 in PBS, then added to the adsorbed Fn patches for 5 h followed by rinsing with PBS buffer. The secondary antibody, (anti-rabbit IgG (Fc specific)-Rhodamine antibody produced in goat, SAB3700846 Sigma), was diluted in PBS (1:200) and then added to the samples and incubated for 1 h, and the biointerface was rinsed with PBS for confocal imaging.

Fluorescence experiments to image the Fn patches were performed using a custom-modified N-SIM (Nikon) microscope with 100× oil immersion objective (NA 1.49). Excitation was done using 561 nm laser diodes (ps) operating on cw mode. The emission light was collected in EMCCD camera through a band-pass filter allowing 570–640 nm light, and images were captured in wide-field mode. The 1000 nm Fn patches were imaged with CLSM using a Zeiss LSM700 CLSM, a 488 nm laser for excitation, and a 63× Plan-Apochromat NA 1.4 objective for visualization.

**DNA-PAINT for Visualizing the Organization of FnBPs on *S. aureus* Cell Membrane.** The DNA-PAINT imaging concept relies on labeling the target molecule with single-stranded DNA, then transient binding of a complementary imager strand which is labeled with a fluorophore induces the blinking phenomena subsequently used to isolate and localize individual fluorophore molecules and reconstruct super-resolution images. Here, we used click chemistry to conjugate a docking DNA strand to Fn via a two-step reaction which involved first labeling the synthesized DNA with NHS-DBCO and then clicking it to Fn prefunctionalized with NHS-azide. The two docking oligos that used in this study (PS3d<sup>67</sup> and R3<sup>68</sup>) are the reversed complement to PS3i and R3i which in turn are used as PAINT imager strands conjugated with Cy3B. The docking oligos were first conjugated with DBCO-NHS-ester, the heterobifunctional linker, at the 5'-amine end (reagents purchased from IDT DK).

**Fn-PEG4-azide Conjugation.** Fn was functionalized with NHS-PEG4-azide by mixing at a 1:10 molar ratio followed by incubation for 5 h at 25 °C with a vortex at 700 rpm in a thermomixer. Unreacted NHS-PEG4-azide was removed using a 100 K Amicon centrifuge filter. The absorption was measured at A<sub>280</sub> to calculate the product concentration. The purified functionalized Fn was verified by sodium dodecyl sulfate-polyacrylamide gel electrophoresis (SDS-PAGE).

**Fn-oligos Conjugation.** Subsequently, the functionalized Fn-EG4-azide in PBS was reacted with DBCO-oligos in a 1:5 ratio followed by incubation for 5 h at 25 °C/700 rpm. The reaction was followed by 100 K Centerfuge Amicon filtration. The spectral measurement was taken at A<sub>280</sub> to calculate the concentration.

**Preparation of *S. aureus* Cells for DNA-PAINT Imaging.** Two protocols for cell immobilization were developed: One was based on biotinylation of the cells followed by immobilization on streptavidin-

**Table 1. Imaging Parameters for DNA-PAINT Images**

image	integration time	frames	laser power	imager concentration	imager	localization precision (NeNA) <sup>69</sup>
Figure 3e	150 ms	30,000	34 mW	5 nM	PS3	12.75 nm
Figure 3f	150 ms	30,000	18.1 mW	5 nM	PS3	15 nm
Figure 4b (right)	200 ms	10,000	110 mW	300 pM	7xR3	9.3 nm
Figure 4b (left)	100 ms	20,000	110 mW	300 pM	7xR3	7 nm
Figure 4c	200 ms	2,000	110 mW	250 pM	7xR3	14 nm

coated ibidi slide, and the other was based on immobilizing cells onto PLL-coated ibidi slides.

**Cell Culture.** One colony of *S. aureus* DSM20231 was inoculated into TSB medium and incubated overnight at 37 °C with shaking at 180 rpm. The OD was adjusted to 0.1 at 600 nm, 1 mL of the culture was centrifuged at 5000×g for 10 min, and the pellet was resuspended and washed three times with PBS.

***S. aureus* Binding with the Functionalized Fibronectin (Fn-PS3d or Fn-R3d).** The functionalized Fn with one of the oligos (PS3d or R3d) were added to *S. aureus* cells to a final concentration of 30 μg/mL in PBS, then the mixture was incubated for 4 h at 25 °C with a vortex at 300 rpm. The mixture was spun down at 5000×g for 10 min, and the pellet was resuspended and washed three times with PBS to remove the excess of (Fn-PS3d or Fn-R3d). The washed pellet was resuspended in ~50 μL of PBS.

**Biotin-Labeling of *S. aureus*.** Three μL of 100 mM biotin-NHS was added to the *S. aureus* in PBS to a final concentration of 5 mM. The mixture was incubated for 15 min at 25 °C with a vortex at 300 rpm. The cell mixture was diluted to 950 μL with PBS to be fixed with 3% PFA + 0.07% glutaraldehyde for 30 min at 37 °C and vortexed at 300 rpm in a thermomixer. Then the reaction was stopped by adding glycine to a final concentration of 15 mM and incubated for 30 min at 25 °C with a vortex at 300 rpm. The mixture was spun down at 2000×g for 10 min, the pellet was resuspended and washed three with PBS, and then the cells pellet was resuspended in 100 μL PBS.

**Slide Preparation. Streptavidin-Coated Channel Slide Preparation.** 60 μL of 1 mg/mL biotin-BSA was added to the ibidi μ-Slide VI 0.5 glass bottom channel slide for 10 min, followed by washing three times with PBS (with 0.05% Tween-20) to remove the unbound biotin-BSA. Then 60 μL of 0.5 mg/mL streptavidin was added to the channel for 10 min, followed by washing three times with PBS (with 0.05% Tween-20) to remove unbound streptavidin.

**Treated *S. aureus* Cells' Immobilization.** 60 μL of *S. aureus* suspension was added onto the channel slide for 30 min before centrifuging the channel slide in a swinging bucket at 3700 rpm for 10 min to spin down the cells onto the surface. The excess cells were removed from the surface by washing three times with PBS. Then 60 μL of 3% BSA was added into the channel for 2 h.

**Alternative Protocol for Cell Immobilization Based on Poly-L-lysine-Coated Ibidi Slides.** The *S. aureus* cells were treated with the functionalized Fn (Fn-PS3d or Fn-R3d) to a final concentration of 30 μg/mL in PBS and incubated for 4 h at 25 °C with a vortex at 300 rpm. The mixture was spun-down at 5000×g for 10 min, and the pellet was resuspended and washed three times with PBS to remove the excess of (Fn-PS3d or Fn-R3d). The washed pellet was resuspended in ~50 μL of PBS. The cells mixture was diluted to 950 μL with PBS to be fixed with 3% PFA + 0.07% glutaraldehyde for 30 min at 37 °C and vortexed at 300 rpm in a thermomixer. The reaction was stopped by adding glycine to a final concentration of 15 mM and incubated for 30 min at 25 °C with a vortex at 300 rpm. The mixture was spun down at 2000×g for 10 min, the pellet was resuspended and washed three with PBS, and then the cells pellet was resuspended in 100 μL PBS.

A PLL (Sigma P8920) solution was diluted first to 1:10 of which 100 μL was added into the ibidi chamber at 4 °C. After 30 min, the channel was rinsed three times with Milli-Q water to remove unbound PLL solution.<sup>62</sup> Then the fixed cells were added into the PLL-coated ibidi chambers for 30 min. The ibidi chamber was centrifuged in the swinging pocket centrifuge at 3700 rpm for 10 min. The non-immobilized cells were removed by rinsing three times with PBS.

**DNA-PAINT Sample Preparation and Imaging.** First, 50 μL of 1:4 AuNPs (~25 μM) was added to the channels and incubated for 15 min. Second, the C-TAD solution was prepared by mixing 380 μL of buffer C (PBS with 0.5 M NaCl, 0.05% Tween-20), 4 μL of 0.1 M Trolox, 10 μL of 0.1 M PCA, and 4 μL of 1 μM PCD. The mixed solution was incubated in the dark for at least 5 min before adding 1 μL of 1 μM the fluorophore-oligo (Cy3B-R3 or Cy3B-PS3 imager strands) to 250 μL of the C-TAD solution to prepare PAINT imaging solution with 4 nM concentration. Eventually, 70 μL imaging solution was added into the chamber's channel.

DNA-PAINT imaging was carried out on an inverted microscope (Nikon Instruments, Eclipse Ti) with the Perfect Focus System, applying an objective-type TIRF configuration equipped with an oil-immersion objective (Nikon Instruments, Apo SR TIRF 100×, NA 1.49, oil). A 561 nm laser (Coherent Sapphire, 200 mW) was used for excitation and was coupled into a single-mode fiber. The laser beam was passed through cleanup filters (Chroma Technology, ZET561/10) and coupled into the microscope objective using a beam splitter (Chroma Technology, ZT561rdc). Fluorescence light was spectrally filtered with an emission filter (Chroma Technology, ET600/50m) and imaged with a sCMOS camera (Andor, Zyla 4.2plus) without further magnification, resulting in an effective pixel size of 130 nm after 2 × 2 binning. The camera readout sensitivity was set to 16-bit and readout bandwidth to 540 MHz.

Imaging parameters for DNA-PAINT images in all figures are provided in Table 1.

**Image Analysis.** Raw fluorescence data from DNA-PAINT imaging were subjected to super-resolution reconstruction using the "Picasso" software package<sup>51</sup> (latest version available on <https://github.com/jungmannlab/picasso>). Drift correction was performed with a redundant cross-correlation and gold nanoparticles as fiducials. DNA-PAINT signal from labeled FnBPs was selected manually using Picasso's "pick tool" and the circle pick option. Density of FnBPs per μm<sup>2</sup> was calculated for circular regions (area 0.36 μm<sup>2</sup> or 0.31 μm<sup>2</sup> the polylysine or streptavidin immobilized bacteria, respectively). Six cells were studied, e.g., as indicated in Figures 3 and 4, giving a range of values. Total number of FnBPs per bacteria was calculated assuming spherical bacteria 1 μm in diameter.

## ASSOCIATED CONTENT

### Supporting Information

The Supporting Information is available free of charge at <https://pubs.acs.org/doi/10.1021/acsnano.2c00630>.

SEM images of the complete range of nanopatterns. Quantification of nanopattern size, coverage and patch spacing. XPS characterization of Al surfaces before and after exposure to media. SIM images of 100 and 200 nm Fn patterns. Fluorescence images and quantification of *S. aureus* adhesions to nanopatterns with a thinner silica layer. SDS gels demonstrating functionalization of FN with DNA oligos (PDF)

Schematic visualization of the sample fabrication process and the bacterial adhesion (MP4)

## AUTHOR INFORMATION

## Corresponding Author

Duncan S. Sutherland – Interdisciplinary Nanoscience Center (iNANO), Aarhus University, Aarhus C 8000, Denmark; [orcid.org/0000-0002-5045-9915](https://orcid.org/0000-0002-5045-9915); Email: [duncan@inano.au.dk](mailto:duncan@inano.au.dk)

## Authors

Heba Khateb – Interdisciplinary Nanoscience Center (iNANO), Aarhus University, Aarhus C 8000, Denmark; [orcid.org/0000-0002-9166-8991](https://orcid.org/0000-0002-9166-8991)

Rasmus S. Sørensen – Interdisciplinary Nanoscience Center (iNANO), Aarhus University, Aarhus C 8000, Denmark

Kimberly Cramer – Max Planck Institute of Biochemistry, Martinsried 82152, Germany

Alexandra S. Eklund – Max Planck Institute of Biochemistry, Martinsried 82152, Germany; [orcid.org/0000-0003-1047-2100](https://orcid.org/0000-0003-1047-2100)

Jorgen Kjems – Interdisciplinary Nanoscience Center (iNANO) and Department of Molecular Biology and Genetics, Aarhus University, Aarhus C 8000, Denmark

Rikke L. Meyer – Interdisciplinary Nanoscience Center (iNANO), Aarhus University, Aarhus C 8000, Denmark

Ralf Jungmann – Max Planck Institute of Biochemistry, Martinsried 82152, Germany; Faculty of Physics and Center for Nanoscience, Ludwig Maximilian University, Munich 80539, Germany; [orcid.org/0000-0003-4607-3312](https://orcid.org/0000-0003-4607-3312)

Complete contact information is available at: <https://pubs.acs.org/10.1021/acsnano.2c00630>

## Author Contributions

H.K. and D.S. conceived and designed the study. H.K. conducted all the surface fabrications, protein engineering, characterization, bioconjugation, and bacterial experiments. H.K., D.S., and R.L.M. contributed to the data interpretation. H.K., K.C., A.K., and R.S. conducted the DNA-PAINT imaging. H.K. and D.S. drafted the manuscript, and all authors commented on the draft manuscript and approved submission.

## Notes

The authors declare no competing financial interest.

## ACKNOWLEDGMENTS

This work was financially supported by the Danmarksgrundforskningsfond center grant DRF135 CellPAT. R.L.M. acknowledges the Carlsberg Foundation grant number CF16-0342 for support.

## REFERENCES

- (1) Centers for Disease Control and Prevention. *Antibiotic resistance threats in the United States*; Centers for Disease Control and Prevention: Atlanta, GA, 2013; pp 11–28.
- (2) Bally, C.; Meyssonier, V.; Bricaire, F. Evolution Of Virulence in Epidemic Community-associated Methicillin-resistant Staphylococcus aureus. *Med. Mal. Infect.* **2011**, *41*, 346–348.
- (3) Pang, Y. Y.; Schwartz, J.; Thoendel, M.; Ackermann, L. W.; Horswill, A. R.; Nauseef, W. M. Agr-dependent Interactions Of Staphylococcus aureus USA300 With Human Polymorphonuclear Neutrophils. *J. Innate Immun.* **2010**, *2*, 546–559.
- (4) Wenzel, R. P. Health Care–Associated Infections: Major Issues in the Early Years of the 21st Century. *Clin. Infect. Dis.* **2007**, *45*, S85–S88.
- (5) World Health Organization. *Report on the Burden of Endemic Health Care-Associated Infection Worldwide; Clean Care is Safer Care*; World Health Organization: Geneva, Switzerland, 2011; pp 1–40.

(6) Kluytmans, J.; Van Belkum, A.; Verbrugh, H. Nasal Carriage of Staphylococcus aureus: Epidemiology, Underlying Mechanisms, and Associated Risks. *Clin. Microbiol. Rev.* **1997**, *10*, 505–520.

(7) Lowy, F. Staphylococcus aureus Infections. *N. Engl. J. Med.* **1998**, *339*, 520–532.

(8) Balasubramanian, D.; Harper, L.; Shopsin, B.; Torres, V. J. Staphylococcus aureus Pathogenesis in Diverse Host Environments. *Pathog. Dis.* **2017**, *75*, ftx005.

(9) Malachowa, N.; Deleo, F. R. Mobile Genetic Elements of Staphylococcus aureus. *Cell. Mol. Life Sci.* **2010**, *67*, 3057–3071.

(10) Thomer, L.; Schneewind, O.; Missiakas, D. Pathogenesis of Staphylococcus aureus Bloodstream Infections. *Annu. Rev. Pathol.* **2016**, *11*, 343–364.

(11) Tong, S. Y. C.; Davis, J. S.; Eichenberger, E.; Holland, T. L.; Fowler, V. G. Staphylococcus aureus Infections: Epidemiology, Pathophysiology, Clinical Manifestations, and Management. *Clin. Microbiol. Rev.* **2015**, *28*, 603–661.

(12) Park, K.-H.; Lee, Y.-M.; Hong, H.-L.; Kim, T.; Park, H. J.; Park, S.-Y.; Moon, S. M.; Chong, Y. P.; Kim, S.-H.; Lee, S.-O.; Choi, S.-H.; Jeong, J.-Y.; Kim, M.-N.; Woo, J. H.; Kim, Y. S. Persistent Catheter-Related Staphylococcus aureus Bacteremia after Catheter Removal and Initiation of Antimicrobial Therapy. *PLoS One* **2012**, *7*, No. e46389.

(13) Cabell, C. H.; Jollis, J. G.; Peterson, G. E.; Corey, G. R.; Anderson, D. J.; Sexton, D. J.; Woods, C. W.; Reller, L. B.; Ryan, T.; Fowler, V. G. Changing Patient Characteristics and the Effect On Mortality In Endocarditis. *Arch. Int. Med.* **2002**, *162*, 90–94.

(14) Tschudin-Sutter, S.; Frei, R.; Dangel, M.; Jakob, M.; Balmelli, C.; Schaefer, D. J.; Weisser, M.; Elzi, L.; Battegay, M.; Widmer, A. F. Validation of a Treatment Algorithm For Orthopaedic Implant-related Infections With Device-retention-results From a Prospective Observational Cohort Study. *Clin. Microbiol. Infect.* **2016**, *22*, 457.e1.

(15) Campoccia, D.; Montanaro, L.; Arciola, C. R. The Significance of Infection Related to Orthopedic Devices and Issues of Antibiotic Resistance. *Biomaterials* **2006**, *27*, 2331–2339.

(16) Kane, T. L.; Carothers, K. E.; Lee, S. W. Virulence Factor Targeting of the Bacterial Pathogen Staphylococcus aureus for Vaccine and Therapeutics. *Curr. Drug Targets* **2018**, *19*, 111–127.

(17) Oliveira, D.; Borges, A.; Simões, M. Staphylococcus aureus Toxins and Their Molecular Activity in Infectious Diseases. *Toxins (Basel)* **2018**, *10*, 252.

(18) Archer, G. L. Staphylococcus aureus: A Well-Armed Pathogen. *Clin. Infect. Dis.* **1998**, *26*, 1179–1181.

(19) Geoghegan, J. A.; Foster, T. J. Cell Wall-Anchored Surface Proteins of Staphylococcus aureus: Many Proteins, Multiple Functions. *Curr. Top. Microbiol. Immunol.* **2015**, *409*, 95–120.

(20) Josse, J.; Laurent, F.; Diot, A. Staphylococcal Adhesion and Host Cell Invasion: Fibronectin-Binding and Other Mechanisms. *Front. Microbiol.* **2017**, *8*, 1–8.

(21) Foster, T. J.; Höök, M. Surface Protein Adhesins of Staphylococcus aureus. *Trends Microbiol.* **1998**, *6*, 484–488.

(22) McCarthy, A. J.; Lindsay, J. A. Genetic Variation in Staphylococcus aureus Surface and Immune Evasion Genes is Lineage Associated: Implications for Vaccine Design and Host-Pathogen Interactions. *BMC Microbiol.* **2010**, *10*, 173.

(23) Pietroccola, G.; Nobile, G.; Alfeo, M. J.; Foster, T. J.; Geoghegan, J. A.; De Fillippis, V.; Speziale, P. Fibronectin-Binding Protein B (FnBPB) from Staphylococcus aureus Protects Against the Antimicrobial Activity of Histones. *J. Biol. Chem.* **2019**, *294*, 3588–3602.

(24) Pollitt, E. J. G.; Szkuta, P. T.; Burns, N.; Foster, S. J. Staphylococcus aureus Infection Dynamics. *PLoS Pathog.* **2018**, *14*, e1007112.

(25) Foster, T. J.; Geoghegan, J. A.; Ganesh, V. K.; Höök, M. Adhesion, Invasion and vasion: The Many Functions of the Surface Proteins of Staphylococcus aureus. *Nat. Rev. Microbiol.* **2014**, *12*, 49–62.

(26) Dziewanowska, K.; Patti, J. M.; Deobald, C. F.; Bayles, K. W.; Trumble, W. R.; Bohach, G. A. Fibronectin Binding Protein and Host Cell Tyrosine Kinase are Required for Internalization of Staph-

- Staphylococcus aureus by Epithelial Cells. *Infect. Immun.* **1999**, *67*, 4673–4678.
- (27) Sinha, B.; Francois, P. P.; Nusse, O.; Foti, M.; Hartford, O. M.; Vaudaux, P.; Froster, S. J.; Lew, D. P.; Herrmann, M.; Krause, B. H. Fibronectin-Binding Protein Acts as Staphylococcus aureus Invasin Via Fibronectin Bridging to Integrin  $\alpha 5 \beta 1$ . *Cell Microbiol.* **1999**, *1*, 101–117.
- (28) Nallapareddy, S. R.; Weinstock, G. M.; Murray, B. E. Clinical Isolates of Enterococcus Faecium Exhibit Strain-Specific Collagen binding Mediated by Acm, a New Member of the MSCRAMM Family. *Mol. Microbiol.* **2003**, *47*, 1733–1747.
- (29) Peacock, S. J.; Foster, T. J.; Cameron, B. J.; Berendt, A. R. Bacterial Fibronectin-Binding Proteins and Endothelial Cell Surface Fibronectin Mediate Adherence of *S. aureus* to Resting Human Endothelial cells. *Microbiology.* **1999**, *145*, 3477–3486.
- (30) Pickering, A. C.; Vitry, P.; Prystopiuk, V.; Garcia, B.; Höök, M.; Schoenebeck, J.; Geoghegan, J. A.; Dufrene, Y. F.; Fitzgerald, J. R. Host-Specialized Fibrinogen-Binding by a Bacterial Surface Protein Promotes Biofilm Formation and Innate Immune Evasion. *PLoS Pathog.* **2019**, *15*, e1007816.
- (31) Henderson, B.; Nair, S.; Pallas, J.; Williams, M. A. Fibronectin: A Multidomain Host Adhesin Targeted by Bacterial Fibronectin-Binding Proteins. *FEMS Microbiol. Rev.* **2011**, *35*, 147–200.
- (32) Schwarz-Linek, U.; Werner, J. M.; Pickford, A. R.; Gurusiddappa, S.; Kim, J. H.; Pilka, E. S.; Briggs, J. A. G.; Gough, T. S.; Hook, M.; Campbell, I. D.; Potts, J. R. Pathogenic Bacteria Attach to Human Fibronectin Through a Tandem b-Zipper. *Nature* **2003**, *423*, 177–181.
- (33) Mongodin, E.; Bajolet, O.; Cutrona, J.; Bonnet, N.; Dupuit, F.; Puchelle, E.; De Bentzmann, S. Fibronectin-Binding Proteins of Staphylococcus aureus are Involved in Adherence to Human Airway Epithelium. *Infect. Immun.* **2002**, *70*, 620–630.
- (34) Speziale, P.; Pietrocola, G. The Multivalent Role of Fibronectin-Binding Proteins A and B (FnBPA and FnBPB) of Staphylococcus aureus in Host Infections. *Front. Microbiol.* **2020**, *11*, 1–13.
- (35) Khalili, A. A.; Ahmad, M. R. A Review of Cell Adhesion Studies for Biomedical and Biological Applications. *Int. J. Mol. Sci.* **2015**, *16*, 18149–18184.
- (36) McCourt, J.; O'Halloran, D. P.; McCarthy, H.; O'Gara, J. P.; Geoghegan, J. A. Fibronectin-Binding Proteins are Required for Biofilm Formation by Community-Associated Methicillin-Resistant Staphylococcus aureus Strain LAC. *FEMS Microbiol. Lett.* **2014**, *353*, 157–164.
- (37) Buck, A. W.; Fowler, V. G.; Yongsunthon, R.; Liu, J.; DiBartola, A. C.; Que, Y.-A.; Moreillon, P.; Lower, S. K. Bonds Between Fibronectin and Fibronectin-Binding Proteins on Staphylococcus aureus and Lactococcus lactis. *Langmuir.* **2010**, *26*, 10764–10770.
- (38) Gautrot, J. E.; Malmström, J.; Sundh, M.; Margadant, C.; Sonnenberg, A.; Sutherland, D. S. The Nanoscale Geometrical Maturation of Focal Adhesions Controls Stem Cell Differentiation and Mechanotransduction. *Nano Lett.* **2014**, *14*, 3945–3952.
- (39) Théry, M. Micropatterning as a Tool to Decipher Cell Morphogenesis and Functions. *J. Cell Sci.* **2010**, *123*, 4201–4213.
- (40) Amin, Y. Y. I.; Runager, K.; Simoes, F.; Celiz, A.; Taresco, T.; Rossi, R.; Enghild, J. J.; Abildtrup, L. A.; Kraft, D. C. E.; Sutherland, D. S.; Alexander, M. R.; Foss, M.; Ogaki, R. Combinatorial Biomolecular Nanopatterning for High-Throughput Screening of Stem-Cell Behavior. *Adv. Mater.* **2016**, *28*, 1472–1476.
- (41) Trappmann, B.; Gautrot, J. E.; Connelly, J. T.; Strange, D. G. T.; Li, Y.; Oyen, M. L.; Cohen Stuart, M. A.; Boehm, H.; Li, B.; Vogel, V.; Spatz, J. P.; Watt, F. M.; Huck, W. T. S. Extracellular-Matrix Tethering Regulates Stem-Cell Fate. *Nat. Mater.* **2012**, *11*, 642–649.
- (42) Cavalcanti-Adam, E. A.; Volberg, T.; Micoulet, A.; Kessler, H.; Geiger, B.; Spatz, J. P. Cell Spreading and Focal Adhesion Dynamics are Regulated by Spacing of Integrin Ligands. *Biophys. J.* **2007**, *92*, 2964–2974.
- (43) Malmström, J.; Christensen, B.; Jakobsen, H. P.; Lovmand, J.; Foldbjerg, R.; Sørensen, E. S.; Sutherland, D. S. Large Area Protein Patterning Reveals Nanoscale Control of Focal Adhesion Development. *Nano Lett.* **2010**, *10*, 686–694.
- (44) Malmström, J.; Lovmand, J.; Kristensen, S.; Sundh, M.; Duch, M.; Sutherland, D. S. Focal Complex Maturation and Bridging on 200 nm Vitronectin But Not Fibronectin Patches Reveal Different Mechanisms of Focal Adhesion Formation. *Nano Lett.* **2011**, *11*, 2264–2271.
- (45) Mao, X.; Kim, J.; Zhang, Q.; Jiang, T.; Ahn, D. O.; Jung, Y.; Matsushita, M.; Bae, T.; Lee, B. L. The N2N3 Domains of C1fA, FnbpA and FnbpB in Staphylococcus aureus Bind to Human Complement Factor H, and Their Antibodies Enhance the Bactericidal Capability of Human Blood. *J. Biochem.* **2021**, *169*, 543–553.
- (46) Hell, S. W.; Wichmann, J. Breaking the Diffraction Resolution Limit by Stimulated Emission: Stimulated-Emission-Depletion Fluorescence Microscopy. *Opt. Lett.* **1994**, *19*, 780.
- (47) Betzig, E.; Patterson, G. H.; Sougrat, R.; Lindwasser, O. W.; Olenych, S.; Bonifacino, J. S.; Davidson, M. W.; Lippincott-Schwartz, J.; Hess, H. F. Imaging Intracellular Fluorescent Proteins at Nanometer Resolution. *Science* **2006**, *313*, 1642–1645.
- (48) Dai, M.; Jungmann, R.; Yin, P. Optical Imaging of Individual Biomolecules in Densely Packed Clusters. *Nat. Nanotechnol.* **2016**, *11*, 798.
- (49) Xu, K.; Babcock, H. P.; Zhuang, X. Dual-Objective STORM Reveals Three-Dimensional Filament Organization in the Actin Cytoskeleton. *Nat. Methods* **2012**, *9*, 185.
- (50) Heilemann, M.; Van De Linde, S.; Schüttelpelz, M.; Kasper, R.; Seefeldt, B.; Mukherjee, A.; Tinnefeld, P.; Sauer, M. Subdiffraction-Resolution Fluorescence Imaging With Conventional Fluorescent Probes. *Angew. Chem., Int. Ed.* **2008**, *47*, 6172–6176.
- (51) Schnitzbauer, J.; Strauss, M. T.; Schlichthaerle, T.; Schueder, F.; Jungmann, R. Super-Resolution Microscopy with DNA-PAINT. *Nat. Protoc.* **2017**, *12*, 1198–1228.
- (52) Eklund, A. S.; Ganji, M.; Gavins, G.; Seitz, O.; Jungmann, R. Peptide-PAINT Super-Resolution Imaging Using Transient Coiled Coil Interactions. *Nano Lett.* **2020**, *20*, 6732–6737.
- (53) Hanarp, P.; Sutherland, D. S.; Gold, J.; Kasemo, B. Control of Nanoparticle Film Structure for Colloidal Lithography. *Colloids Surf., A* **2003**, *214*, 23–36.
- (54) Jungmann, R.; Avendano, M. S.; Woehrstein, J. B.; Dai, M.; Shih, W. M.; Yin, P. Multiplexed 3D Cellular Super-Resolution Imaging with DNA-PAINT and Exchange-PAINT. *Nat. Methods* **2014**, *11*, 313–318.
- (55) Jungmann, R.; Steinhauer, C.; Scheible, M.; Kuzyk, A.; Tinnefeld, P.; Simmel, F. C. Single-Molecule Kinetics and Super-Resolution Microscopy by Fluorescence Imaging of Transient Binding on DNA Origami. *Nano Lett.* **2010**, *10*, 4756–4761.
- (56) Haynes, C. L.; Van Duyne, R. P. Nanosphere Lithography: A Versatile Nanofabrication Tool for Studies of Size-Dependent Nanoparticle Optics. *J. Phys. Chem. B* **2001**, *105*, 5599–5611.
- (57) Malmström, J.; Agheli, H.; Kingshott, P.; Sutherland, D. S. Viscoelastic Modeling of Highly Hydrated Laminin Layers at Homogeneous and Nanostructured Surfaces: Quantification of Protein Layer Properties Using QCM-D and SPR. *Langmuir* **2007**, *23*, 9760–9768.
- (58) Andersen, A. S.; Aslan, H.; Dong, M.; Jiang, X.; Sutherland, D. S. Podosome Formation and Development in Monocytes Restricted by the Nanoscale Spatial Distribution of ICAM1. *Nano Lett.* **2016**, *16*, 2114–2121.
- (59) Casolini, F.; Visai, L.; Joh, D.; Conaldi, P. I.; Toniolo, A.; Höök, M.; Speziale, P. Antibody Response to Fibronectin-Binding Adhesin FnbpA in Patients with Staphylococcus aureus Infections. *Infect. Immun.* **1998**, *66*, 5433–5442.
- (60) Spengler, C.; Thewes, N.; Jung, P.; Bischoff, M.; Jacobs, K. Determination of the Nano-scaled Contact Area of Staphylococcal Cells. *Nanoscale* **2017**, *9*, 10084–10093.
- (61) Bingham, R. J.; Rudino-Pinera, E.; Meenan, N. A. G.; Schwarz-Linek, U.; Turkenburg, J. P.; Hook, M.; Garman, E. F.; Potts, J. R. Crystal Structures of Fibronectin-Binding Sites From Staphylococcus aureus FnBPA in Complex With Fibronectin Domains. *Proc. Natl. Acad. Sci. U. S. A.* **2008**, *105*, 12254–12258.
- (62) Stockmar, I.; Feddersen, H.; Cramer, K.; Gruber, S.; Jung, K.; Bramkamp, M.; Shin, J. Y. Optimization of Sample Preparation and

Green Color Imaging Using the mNeonGreen Fluorescent Protein in Bacterial Cells for Photoactivated Localization Microscopy. *Sci. Rep.* **2018**, *8*, 1–11.

(63) Tokunaga, M.; Imamoto, N.; Sakata-Sogawa, K. Highly Inclined Thin Illumination Enables Clear Single-Molecule Imaging in Cells. *Nat. Methods* **2008**, *5*, 159–161.

(64) Lower, S. K.; Yongsunthon, R.; Casillas-Ituarte, N. N.; Taylor, E. S.; DiBartola, A. C.; Lower, B. H.; Beveridge, T. J.; Buck, A. W.; Fowler, V. G. A Tactile Response in *Staphylococcus aureus*. *Biophys. J.* **2010**, *99*, 2803–2811.

(65) Kerdudou, S.; Laschke, M. W.; Sinha, B.; Priessner, K. T.; Menger, M. D.; Herrmann, M. Fibronectin Binding Proteins Contribute to the Adherence of *Staphylococcus aureus* to Intact Endothelium In Vivo. *Thromb. Haemost.* **2006**, *96*, 183–189.

(66) Shiroma, A.; Terabayashi, Y.; Nakano, K.; Shimoji, M.; Tamotsu, H.; Ashimine, N.; Ohki, S.; Shinzato, M.; Teruya, K.; Satou, K.; Hirano, T. First Complete Genome Sequences of *Staphylococcus aureus* Subsp. *aureus* Rosenbach 1884 (DSM 20231T), Determined by PacBio Single-Molecule Real-Time Technology. *Genome Announc.* **2015**, *3*, e00800.

(67) Schueder, F.; Stein, J.; Stehr, F.; Auer, A.; Sperl, B.; Strauss, M. T.; Schwille, P.; Jungmann, R. An Order of Magnitude Faster DNA-PAINT Imaging by Optimized Sequence Design and Buffer Conditions. *Nat. Methods* **2019**, *16*, 1101–1104.

(68) Strauss, S.; Jungmann, R. Up to 100-fold Speed-Up and Multiplexing in Optimized DNA-PAINT. *Nat. Methods* **2020**, *17*, 789–791.

(69) Endesfelder, U.; Malkusch, S.; Fricke, F.; Heilemann, M. A Simple Method to Estimate the Average Localization Precision of a Single-Molecule Localization Microscopy Experiment. *Histochem. Cell Biol.* **2014**, *141*, 629–638.